Detecting Intramolecular Dynamics and Multiple Förster Resonance Energy Transfer States by Fluorescence Correlation Spectroscopy

E. Shane Price, Matthew S. DeVore, and Carey K. Johnson*

Department of Chemistry, University of Kansas, Lawrence, Kansas 66045

Received: December 23, 2009; Revised Manuscript Received: March 18, 2010

Fluorescence correlation spectroscopy (FCS) is a robust method for the detection of intramolecular dynamics in proteins but is also susceptible to interference from other dynamic processes such as triplet kinetics and photobleaching. We describe an approach for the detection of intramolecular dynamics in proteins labeled with a FRET dye pair based on global fitting to the two autocorrelation functions (green−green and red−red) and the two cross-correlation functions (green−red and red−green). We applied the method to detect intramolecular dynamics in the Ca^{2+} signaling protein calmodulin. Dynamics were detected on the 100 μs time scale in Ca^{2+}-activated calmodulin, whereas in apocalmodulin dynamics were not detected on this time scale. Control measurements on a polyproline FRET construct (Gly-Pro_{15}-Cys) demonstrate the reliability of the method for isolating intramolecular dynamics from other dynamic processes on the microsecond time scale and confirm the absence of intramolecular dynamics of polyproline. We further show the sensitivity of the initial amplitudes of the FCS auto- and cross-correlation functions to the presence of multiple FRET states, static or dynamic. The FCS measurements also show that the diffusion of Ca^{2+}-calmodulin is slower than that of apocalmodulin, indicating either a larger average hydrodynamic radius or shape effects resulting in a slower translational diffusion.

Introduction

Fluorescence correlation spectroscopy (FCS) reveals fluctuations in the fluorescence intensity of a small number of molecules as they pass through the probe volume. FCS detects both concentration fluctuations within the focal volume and kinetic or photophysical processes such as triplet population kinetics and fluorescence quenching. An early application of FCS was to chemical kinetics.[1,2] For biological systems,[3−7] important applications of FCS include reaction kinetics,[2,8−11] conformational dynamics[12−14] high-throughput assays,[6,15−17] intracellular dynamics,[18,19] and a host of others.

Introduction of donor and acceptor fluorophores into the same protein molecule brings in the possibility of fluctuations in the fluorescence intensity through Förster resonance energy transfer (FRET). FCS with FRET is a powerful combination for probing molecular conformations and dynamics, as illustrated by a number of recent publications.[11,14,20−26] FRET states may be *static*, that is, involving interchange between FRET states that is slow on the time scale of diffusion through the detection volume, or *dynamic*, leading to fluctuations in fluorescence on the time scale of the molecules transit through the focal region. Methods are needed to analyze FCS data to clearly and reliably distinguish FRET dynamics from other sources of fluctuations. Triplet state dynamics, for example, often occur on the microsecond time scale, and their contribution must be clearly distinguishable from intramolecular dynamics.

In this paper, we examine the relationship between FCS and FRET in two systems, one with dynamics on the time scale of transit through the focal region and another where dynamics occur on time scales much faster (or slower) than but not on the time scale as transit through the focal region. In the first system, we expect contributions to FCS auto- and cross-correlations from intramolecular dynamics. In the second (nondynamic) system, we expect FRET states to be static on the FCS time scale. Satisfactory fitting of FCS curves for a nondynamic system will serve as a control for FCS curves in cases where dynamics may be present.

A system with static FRET states on the microsecond time scale is polyproline with length ranging from 6 to 20 prolines.[27−30] Using a polyproline sample labeled with donor and acceptor fluorophores, we show that the amplitudes of the FCS correlation functions, both autocorrelations and cross-correlations, are sensitive to the presence of multiple FRET states. Furthermore, analysis of the time dependence confirms the absence of dynamics on the time scale of transit through the focal region. We compare these results with FCS of calmodulin (CaM), a system where we have previously detected dynamics on the microsecond time scale.[31] We compute the two autocorrelation functions, one for the green channel and one for the red channel, and the two cross-correlation functions. Our strategy for finding FRET dynamics in CaM is to fit the four functions globally, tying parameters (diffusion time, dynamics time constant, average molecule number, etc.) across all four fits.

Materials and Methods

Sample Preparation. A synthetic peptide with the sequence Gly-$(Pro)_{15}$-Cys was purchased from Sigma Genosys (St. Louis, MO). The amino terminal glycine and carboxyl terminal cysteine were positioned to allow conjugation of reactive fluorescent dyes to the respective sites. Lyophilized peptide was dissolved in 50 mM sodium phosphate buffer at pH 7.2 and labeled with Texas Red (TR) maleimide (Invitrogen Corp., Carlsbad, CA) as per manufacturer recommendations. The labeled peptide was purified on a Superdex Peptide HR 10/30 size exclusion column (GE Healthcare Life Sciences) with 20 mM sodium bicarbonate buffer at pH 7.5. The collected fractions were then concentrated

* To whom correspondence should be addressed. E-mail: ckjohnson@ku.edu.

10.1021/jp912125z
Published on Web 04/14/2010

to ~0.25 mM and dialyzed into 100 mM sodium bicarbonate buffer at pH 7.5. Reaction of the amino terminus was carried out with Alexa Fluor 488 (AF488) succinimidyl ester (Invitrogen Corp.) at room temperature for 90 min. The doubly labeled peptide was purified on the Superdex Peptide HR 10/30 size exclusion column as described above. Samples were verified to consist of pure donor−acceptor-labeled peptide by mass spectrometry and UV−vis absorbance measurements.

CaM with two threonine to cysteine mutations (T34C, T110C-CaM) was expressed and labeled with AF488 maleimide and TR maleimide as described previously.[32] CaM doubly labeled with donor and acceptor was separated from other species (double-donor, double-acceptor, etc.) by high-performance liquid chromatography as described previously.[33]

FCS Measurements. FCS measurements were performed on an inverted fluorescence microscope (Nikon TE2000) adapted for two-color FCS measurements. Laser light at 488 nm from an argon ion laser source (JDS Uniphase) was made circularly polarized with a $\lambda/4$ waveplate and passed through a 488/10x excitation filter (Chroma Technology Corp., Rockingham, VT). The light was reflected into a 60× water-immersion objective (UPLSAPO, Olympus, Center Valley, PA) by a 500DCXR dichroic mirror (Chroma). For polyproline measurements, a sample of ~30 μL of a 5 nM solution in pH 7.0 sodium phosphate buffer was placed on a coverslip treated with bovine serum albumin to reduce sample loss due to adhesion of protein to the surface. For high Ca^{2+} conditions, CaM was added to a pH 7.4 buffer consisting of 10 mM HEPES, 0.1 M KCl, 1 mM $MgCl_2$, and 0.1 mM $CaCl_2$. The low Ca^{2+} buffer was prepared with 10 mM HEPES, 100 mM KCl, 1 mM $MgCl_2$, and 3 mM EGTA and adjusted to pH 7.4. The concentration of each sample was adjusted to give correlation curves with initial amplitudes in the range of 0.2−1.0. This generally resulted in concentrations of 10−20 nM for each sample.

The laser focus was positioned 20 μm above the surface of the coverslip. Fluorescence was collected in an epifluorescence arrangement and passed through the dichroic mirror. The fluorescence was split into green and red components by a 565DCLP dichroic beam splitter (Chroma). Pinholes (75 μm) were placed in each of the beam paths at their image planes. Separate pinholes for each channel were necessary for optimum probe volume overlap to correct for chromatic aberrations in the microscope optics. The fluorescence transmitted through the pinholes was focused onto the active area of the single-photon counting modules (Perkin-Elmer SPCM AQR-14). Emission filters were placed in front of the green (HQ535/50 M Chroma) and red (HQ620/75 M Chroma) detectors. The resulting stream of photon counts was collected for approximately 5 min with a PCI-6602 counter timer card (National Instruments, Austin, TX) controlled with LabView software to tag photon arrival times of both channels using the on-board 80-MHz clock.

Correlation Functions. Correlation functions were calculated from photon arrival times with a quasi-logarithmic time axis as described by previous workers.[34−37] After-pulsing correction was applied by the method of Zhao et.al.[38] Briefly, after-pulsing profiles were collected by focusing to the surface of a coverslip and collecting laser scatter at approximately a 1 kHz count rate for each channel for about 1 million photon counts. The after-pulsing files were correlated and converted to a probability distribution. The probability distributions were fit to a multiple exponential function chosen to accurately describe the shape of the after-pulse contribution starting at the peak of the after-pulse. The resulting fit parameters were then used to subtract the after-pulsing contribution from the collected data sets.

Autocorrelation functions were fit to equations of the form

$$G_{xx}(\tau) = \frac{1}{N_{tot}} G_T(\tau)\, G_{diff}(\tau)\, E_{xx}(\tau) \qquad (1)$$

where the subscript x denotes the green (G) or red (R) channel, $E_{xx}(\tau)$ is the contribution from intramolecular dynamics (defined in greater detail below), and $G_T(\tau)$ is the triplet contribution given by:[39]

$$G_T(\tau) = \frac{(1 - f_T) + f_T e^{-\tau/\tau_T}}{(1 - f_T)}$$

where f_T is the amplitude for the triplet component and τ_T is the triplet time constant, N_{tot} is the average number of fluorescent molecules in the focal volume, and $G_{diff}(\tau)$ is given by:

$$G_{diff}(\tau) = \left(1 + \frac{\tau}{\tau_d}\right)^{-1}\left(1 + \frac{\tau}{p^2\tau_d}\right)^{-1/2} \qquad (2)$$

The axial−radial ratio p was determined previously to equal 8 for our system[31] and was fixed for data fitting. Cross-correlation functions were fit to a similar correlation decay function but without the triplet component:

$$G_{xy}(\tau) = \frac{1}{N_{tot}} G_{diff}(\tau)\, E_{cc}(\tau) \qquad (x \neq y) \qquad (3)$$

where $E_{cc}(\tau)$ is the contribution to the cross-correlation from intramolecular dynamics. Global fits were carried in Microsoft Excel using the built-in solver to minimize the sum of χ^2 values over the four data sets. To calculate the appropriate weighting to use in the fits, each data file for CaM FCS curves was split into eight equal sections.[40] The correlations were calculated for each of the eight sections, and the variance σ^2 for each correlation point was determined. In fits, each point in the correlation function was weighted by $1/\sigma^2$.

Theory

In this section, we present a theoretical description of the FCS autocorrelation and cross-correlation functions generated by a system (static or dynamic) with multiple FRET states. Four correlation functions can be calculated from the green and red data streams:

$$G_{xy}(\tau) = \frac{\langle \delta I_x(t)\, \delta I_y(t + \tau)\rangle}{\langle \delta I_x(t)\rangle\langle \delta I_y(t)\rangle} \qquad (4)$$

where x and y are the green or red signal channels and $\langle\cdots\rangle$ denotes the average over t. For green (G) and red (R) fluorescence channels, eq 4 gives two autocorrelation functions (xy = GG, RR) and two cross-correlation functions (xy = GR, RG).

Case of Static FRET States. If the FRET efficiency is static on the FCS time scale (microseconds to milliseconds in this case), then the presence of multiple FRET states affects only the initial amplitudes but not the time dependence of the correlation functions. With fractional populations of FRET states f_i (written here for i = 1, 2), the initial amplitudes of the

correlation functions (not including contributions from processes other than diffusion, such as triplet kinetics or photon antibunching) can be written[41]

$$G_{GG}(0) = \frac{1}{N_{tot}}\left[\frac{(1-E_1)^2 f_1 + (1-E_2)^2(1-f_1)}{[(1-E_1)f_1 + (1-E_2)(1-f_1)]^2}\right] \quad (5)$$

$$G_{RR}(0) = \frac{1}{N_{tot}}\left[\frac{\gamma_1^2 f_1 + \gamma_2^2(1-f_1)}{[\gamma_1 f_1 + \gamma_2(1-f_2)]^2}\right] \quad (6)$$

$$G_{GR}(0) = \frac{1}{N_{tot}}\left[\frac{(1-E_1)\gamma_1 f_1 + (1-E_2)\gamma_2(1-f_1)}{[(1-E_1)f_1 + (1-E_2)(1-f_1)][\gamma_1 f_1 + \gamma_2(1-f_1)]}\right] \quad (7)$$

where N_{tot} is the average total number of molecules in the focal volume, E_i is the FRET efficiency for conformational state i, and $\gamma_i = [\beta E_i + (1-E_i)\alpha]$, where β is the brightness factor of the FRET-excited acceptor relative to the directly excited donor and α is the fractional contribution of cross-talk of donor emission into the acceptor channel. Equations 5−7 assume that the quantum yields of donor and acceptor are independent of the FRET state. (We have also assumed that there is no direct excitation of acceptor, although correction for it could easily be incorporated as well.) These expressions are readily extended to any number of static FRET states in an obvious way. Similar equations for a static FRET system were derived previously in the Gratton group for the case of a single FRET state in the presence of species labeled with donor only and acceptor only.[42]

Equations 5−7 predict the dependence of the initial amplitudes of correlation functions on the FRET efficiencies of the states present. If only a single FRET state exists ($f_1 = 1$), the initial amplitudes predicted by eqs 5−7 are identical and given by $1/N_{tot}$. The result (apart from other processes such as triplet kinetics) would be overlapping correlation decay curves. In the presence of two or more static FRET states, the initial amplitudes are no longer equal. Thus, the initial amplitudes of the auto- and cross-correlation functions for a FRET system can be used to diagnose the presence of multiple FRET states. If their FRET efficiencies are known in advance, the initial amplitudes can then be used to determine the populations of each of these states.

Case of Dynamic FRET States. In the case of dynamic FRET states, the FRET efficiency can change while a molecule diffuses through the probe volume. The resulting fluorescence fluctuations lead to additional decay (for the autocorrelations) or rise (for cross-correlations) components. Expressions have been derived for correlation functions with dynamic interchange between FRET states.[25,42−46] For interchange between two FRET states with FRET efficiencies E_1 and E_2

$$E_1 \underset{k_{-1}}{\overset{k_1}{\rightleftharpoons}} E_2$$

the FCS correlation functions can be written[14,25,42,44]

$$G_{GG}(\tau) = G_T(\tau)\, G_{diff}(\tau)\left[1 + \frac{f_1 f_2 (E_1 - E_2)^2}{(1 - f_1E_1 - f_2E_2)^2}\, e^{-\tau/\tau_1}\right] \quad (8)$$

$$G_{RR}(\tau) = \frac{1}{N_{tot}}\, G_T(\tau)\, G_{diff}(\tau) \times \left[1 + \frac{f_1 f_2 (E_1 - E_2)^2(\beta - \alpha)^2}{[\beta(f_1E_1 + f_2E_2) + \alpha(1 - f_1E_1 - f_2E_2)]^2}\, e^{-\tau/\tau_1}\right] \quad (9)$$

$$G_{GR}(\tau) = G_{RG}(\tau) = \frac{1}{N_{tot}}\, G_{diff}(\tau) \times \left[1 - \frac{f_1 f_2 (E_1 - E_2)^2(\beta - \alpha)}{\beta(1 - f_1E_1 - f_2E_2)(f_1E_1 + f_2E_2) + \alpha(1 - f_1E_1 - f_2E_2)^2}\, e^{-\tau/\tau_1}\right] \quad (10)$$

where $G_T(\tau)$ is the triplet contribution and $\tau_1 = (k_1 + k_{-1})^{-1}$ is the kinetic relaxation time. We have assumed that both the quantum efficiencies of the fluorophores and the diffusion coefficients are the same in the two FRET states and therefore unchanged by conformational changes of the protein. We note that apart from the triplet contribution, eqs 8−10 reduce to eqs 5−7 at $\tau = 0$.

Results

Probe Volume Overlap. To correctly measure auto and cross-correlation functions, the two channels (green and red) must detect the same region of the sample. Overlap of the detection volumes probed in the green and red channels was verified with fluorescence from CaM-34-110 doubly labeled with AF488 (CaM-AF488-AF488), which was detected in both channels. The signal in the red channel arose from cross-talk of fluorescence into the red channel (about 15%). CaM-AF488-AF488 emission with cross-talk replicates a FRET system with a single FRET efficiency. The two autocorrelation functions, $G_{GG}(\tau)$ and $G_{RR}(\tau)$, and the two cross-correlation functions, $G_{GR}(\tau)$ and $G_{RG}(\tau)$, were calculated. Figure 1 shows the four correlation functions for CaM-AF488-AF488. The overlap of the four correlation curves demonstrates overlap of the probe volumes for the green and red channels.

FCS of Polyproline FRET Pair. After verification of the probe volume overlap as described above, data were recorded for the peptide Gly-$(Pro)_{15}$-Cys labeled with donor and acceptor fluorophores AF 488 and TR (polyproline-AF488-TR). The four

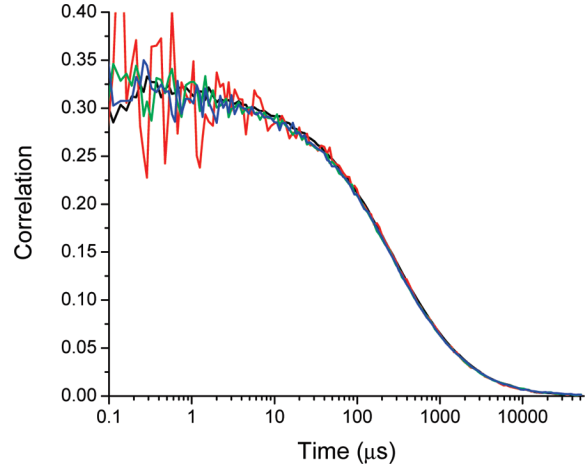

Figure 1. Correlations for CaM-AF488-AF488: $G_{GG}(\tau)$ (black), $G_{RR}(\tau)$ (red), $G_{GR}(\tau)$ (green), and $G_{RG}(\tau)$ (blue). The signal in the red channel arises from AF488 fluorescence detected in the red channel. The close overlap of all four correlation functions demonstrates proper alignment of the probe volumes for the two channels.

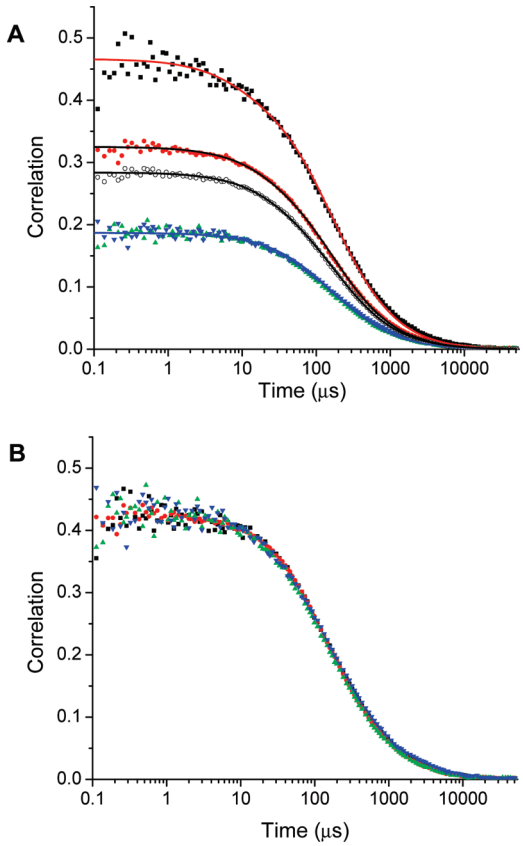

Figure 2. (A) Correlation functions for polyproline-AF488-TR: $G_{GG}(\tau)$ (black squares), $G_{RR}(\tau)$ (red circles), $G_{GR}(\tau)$ (green triangles), and $G_{RG}(\tau)$ (blue inverted triangles). The open circles show the correlation of the combined photon stream. The solid lines show a global fit where the transit times are linked [for $G_{GG}(\tau)$, $G_{GR}(\tau)$, and $G_{RG}(\tau)$], and the initial amplitudes are allowed to vary independently. Fitting parameters are in Table 1. (B) Correlation functions for polyproline-AF488-TR normalized to show overlap of the time dependence of the four correlation functions.

correlation functions are shown in Figure 2. Unlike the correlation functions for CaM-AF488-AF488 in Figure 1, the correlation functions for polyproline-AF488-TR do not overlay each other. The two cross-correlations $G_{GR}(\tau)$ and $G_{RG}(\tau)$ overlap as expected but have an initial amplitude different from those of the two autocorrelations $G_{GG}(\tau)$ and $G_{RR}(\tau)$, which themselves have different amplitudes. The four correlation functions were fit globally to eq 1 or eq 3 without intramolecular dynamics with a total of eight fitting parameters (the triplet parameters f_T and τ_T for green and red channels, the three initial amplitudes, and the diffusion time τ_d). The initial amplitudes $G_{xy}(0)$ served as fitting parameters, while the transit time was fit globally over all four correlation functions (Figure 2A). Triplet decay components were included in fits to the two autocorrelation functions but not in the fits to the cross-correlation functions. Table 1 shows the average values and standard errors for the fitting parameters from three separate data sets. Global fitting imposes significant constraints on the fitting parameters as suggested by the reproducibility of the fits across the three data sets.

Our purpose in analyzing the correlation functions of polyproline-AF488-TR was to verify that the time dependences of the autocorrelation and cross-correlation functions are identical in FCS measurements for a molecule with no dynamics on the microsecond to millisecond time scales (after correction for after-pulsing and triplet contributions). Figure 2B shows the four

TABLE 1: Global Fit Parameters for Polyproline Averaged from Different Days[a]

	average	standard error[b]
f_T (green)	0.081	0.009
τ_T (green) (μs)	11.4	3.6
f_T (red)	0.065	0.010
τ_T (red) (μs)	19.2	1.1
$G_{GG}(0)$	0.403	0.015
$G_{RR}(0)$	0.273	0.018
$G_{GR}(0)$ and $G_{RG}(0)$	0.165	0.010
τ_D (μs)	158.2	6.0
p (fixed)	8	

[a] The initial amplitudes were allowed to vary independently. [b] Standard deviation of the mean of three measurements.

correlations normalized to the same initial values. The normalization was performed by first dividing out the triplet contributions from the two autocorrelations and then using the initial amplitudes from the global fit to scale all of the correlations to the same initial value. The overlap demonstrates the identical time dependence of the four correlation functions and thus the absence of intramolecular dynamics on the microsecond to millisecond time scales. If there were fluctuations in the FRET efficiency on the microsecond to millisecond time scale, then two extra features would be present. First, the two autocorrelations would have an additional decay component due to another source of fluctuations in the fluorescence signal (eqs 8 and 9). Second, the cross-correlations would contain a rising component due to the anticorrelated nature of FRET fluctuations between the two channels (eq 10). FRET fluctuations would therefore result in the normalized curves not overlapping as they do in Figure 2. The successful fits to the polyproline correlation functions without an intramolecular dynamics component confirm the absence of dynamics on the microsecond time scale.

The different initial amplitudes of the correlation functions are observed in Figure 2, even after correction for after-pulsing and triplet decay. The sample was known to consist of pure donor−acceptor-labeled peptide, eliminating the possibility of a difference in initial amplitudes caused by a difference in the concentrations of the two fluorophores present. Thus, the initial amplitudes demonstrate the presence of more than one FRET efficiency in the polyproline sample or of polyproline molecules without an active acceptor. Equations 5−7 provide the simplest model (two FRET states with the FRET parameters E_1, E_2, and f_1 and the molecule number N_{tot}) to describe the initial amplitudes. The initial amplitudes constitute three constraints on these parameters. Thus, the initial amplitudes of the green autocorrelation $G_{GG}(0)$, the red autocorrelation $G_{RR}(0)$, and the two cross-correlations $G_{GR}(0)$ and $G_{RG}(0)$, which have the same initial amplitude apart from experimental noise, can be used to determine three parameters. The absolute scale of the initial amplitudes is determined by the molecule number N_{tot}. The three FRET parameters E_1, E_2, and f_1 determine the relative signal levels in the green and red channels and thus are associated with the relative values of the initial amplitudes. It follows that the three values of the initial amplitudes can be used to determine the molecule number N_{tot} and two of the FRET parameters. Equations 5−7 thus yield the value of N_{tot} and ranges of values for E_1, E_2, and f_1 consistent with the measured initial amplitudes. The following range of values is consistent with the initial amplitudes for polyproline in Table 1: $N_{tot} = 4.2$, $0.79 \leq E_1 \leq 0.94$, $0.04 \leq E_2 \leq 0.37$, and $0.44 \leq f_1 \leq 0.80$.

The average molecule number N_{tot} can also be estimated from the combined photon stream from the two channels. For the

case where the quantum yields and detection efficiencies of the two fluorophores are equal, the result is a data stream with the effect of FRET removed. In the present case, the quantum yields and detection efficiencies differ by only 10% for the two dyes, so the effect of FRET should be largely absent from the autocorrelation function for the combined photon stream. The autocorrelation of the combined photon stream is included in Figure 2. The combined correlation was fit with a single diffusion time and a triplet component (eq 1). The average total number of particles in the focal volume N_{tot} was then determined from the initial amplitude of the fit, and the value (4.2) is in very good agreement with the value determined from the individual correlation amplitudes.

Given the unequal initial amplitudes, we now address the question of the nature of the multiple FRET states. To identify FRET states that were detected by FCS, single-molecule burst measurements of the polyproline sample were carried out following methods described previously.[47] The resulting histogram of the apparent FRET efficiencies displays a population with FRET efficiency greater than 0.7 and another with apparent FRET efficiency less than 0.2 (see the Supporting Information). The average FRET efficiency in the range $E > 0.4$ was 0.82 (fraction 0.74), and the average FRET efficiency for $E < 0.4$ was 0.12 with a fraction of 0.26. The burst measurements are consistent with parameters values obtained from solution of eqs 5−7. Thus, the initial amplitudes can be predicted from the FRET efficiencies of the states present. Furthermore, the initial amplitudes could be used to determine the FRET parameters or populations in appropriate systems. For example, if the FRET efficiencies were known from independent measurements, the initial amplitudes of the four correlation functions could be used to find the fractional populations and the total number of molecules.

A population with a low apparent FRET efficiency was detected both in the burst distributions and by analysis of the FCS initial amplitudes. However, an apparent FRET efficiency of ca. 0.1 is inconsistent with the predicted FRET efficiency for a straight chain polyproline conformation (end-to-end distance of ≤42 Å[28] or FRET efficiency >0.7), suggesting that this population was most likely a result of photobleaching of the acceptor molecule. Because molecules that pass through the focal volume have a significant probability of re-entry into the observation volume in FCS and burst measurements,[48] photobleaching generates fluorescence bursts with a low apparent FRET efficiency. Thus, we expect that the population with low apparent FRET efficiency arose from molecules with a photobleached acceptor fluorophore.

FCS of CaM. In contrast to polyproline, CaM is a molecule where dynamics are expected on the microsecond time scale.[31] Correlation functions for CaM-34-110 labeled with AF488 and TR (CaM-AF488-TR) are shown in Figure 3 for high Ca^{2+} and low Ca^{2+} conditions. For both Ca^{2+}-CaM and apoCaM, it was necessary to include a static FRET component to describe the correlation decays. To model this data, the correlation functions for three interchanging FRET states were derived (see the Supporting Information). In the limit where one time constant is long compared to the transit time, the intramolecular FRET fitting functions take the form:

$$\begin{aligned} E_{GG}(\tau) &= 1 + ae^{-t/\tau_1} + b \\ E_{RR}(\tau) &= 1 + ce^{-t/\tau_1} + d \\ E_{GR}(\tau) &= E_{RG}(\tau) = 1 - \sqrt{ac}e^{-t/\tau_1} - \sqrt{bd} \end{aligned} \quad (11)$$

where a and c are the amplitudes for dynamic FRET and b and d are the amplitudes for static FRET. These parameters can be defined in terms of the kinetic rate constants and FRET efficiencies of the FRET states (see the Supporting Information). The four correlation functions for Ca^{2+}-CaM were fit globally with the eight fitting parameters in Table 2 plus the four amplitude parameters (a, b, c, and d) in eq 11. Of these fitting parameters, the triplet parameters were fixed to the values previously determined for polyproline, leaving eight adjustable parameters that were determined from the global fits over four correlation functions. For apoCaM, the fitting parameters to describe dynamic FRET (a, c, and τ) were not needed. Transit times for both sets of correlations were linked for $G_{GG}(\tau)$, $G_{GR}(\tau)$, and $G_{RG}(\tau)$, but a shorter transit time was used for $G_{RR}(\tau)$ to account for a small contribution to the time dependence from photobleaching of the acceptor fluorophore.

Table 2 lists the fitting parameters for each of the samples. The fits reveal a correlation time of ∼90 μs for intramolecular dynamics in Ca^{2+}-CaM. FRET dynamics were not detectable for apoCaM. The triplet parameters τ_T and f for $G_{GG}(\tau)$ were set to values obtained from CaM doubly labeled with AF 488 (CaM-AF488-AF488) and fixed during fitting. For TR, the triplet parameters were taken from fits to the polyproline $G_{RR}(\tau)$ autocorrelation decays. The triplet parameter values depend on laser power and therefore were determined using the same laser powers used for the measurements of CaM. The time scale for dynamics is in agreement with the value previously reported from our laboratory,[31] but the amplitude of the dynamics reported here is smaller. This appears to be a result, at least in part, of an irregular response in the control of the NI-6602 data collection card used for the previous measurements, which affected the cross-correlation functions. This problem was rectified for the present measurements. To aid in visualizing the presence or absence of dynamics, the correlations are also shown normalized (Figure 3C,D). The high Ca^{2+} CaM 34-110 correlations clearly show dynamics on the 100s of μs time scale, whereas overlap of the curves for apoCaM shows that dynamics were not detected in the low Ca^{2+} buffer.

The parameters summarized in Table 2 indicate a longer transit time for Ca^{2+}-CaM than for apoCaM. To check this result, the transit times were determined independently from the autocorrelation function for CaM-AF488-AF488, where the only dynamics contributions come from diffusion and triplet blinking. Figure 4 shows the correlation results for CaM-AF488-AF488. The transit times τ_d for CaM-AF488-AF488 differed in the high Ca^{2+} ($\tau_d = 297 \pm 10$ μs) and low Ca^{2+} ($\tau_d = 267 \pm 8$ μs) buffers, in agreement with the value for τ_d in Table 2. The difference in τ_d for the high and low Ca^{2+} buffers was reproducible and was not a result of changes to the buffer viscosity, as shown by the fact that the transit times of free AF488 dye was 65 ± 3 and 64 ± 3 μs for the high and low Ca^{2+} buffers, respectively. The relative transit times of CaM at high and low Ca^{2+} corresponds to a roughly 10% higher hydrodynamic radius at high Ca^{2+}. This difference was not resolved in our previous FCS measurements on CaM.[31] However, shape differences could also contribute to the difference in transit time.

Discussion

The propensity of CaM to recognize and bind many different target peptide sequences[49−51] suggests that CaM is a particularly flexibile and dynamic protein. Dynamics are necessary for protein function. Hence, we expect that CaM dynamics involved in Ca^{2+} binding or in recognition and binding to an enzyme

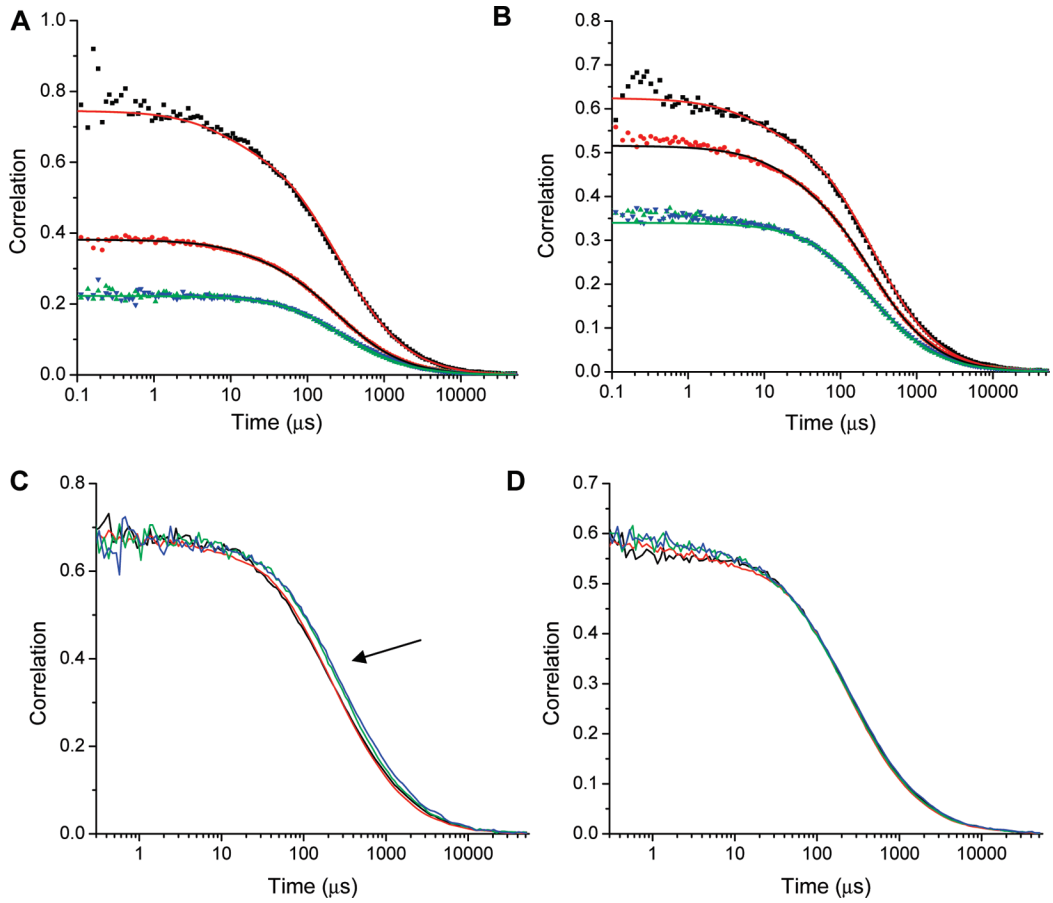

Figure 3. Correlation functions for CaM-AF488-TR. (A) CaM in high-Ca^{2+} buffer: $G_{GG}(\tau)$ (black squares), $G_{RR}(\tau)$ (red circles), $G_{GR}(\tau)$ (green triangles), and $G_{RG}(\tau)$ (blue inverted triangles). The solid lines show a global fit with a time constant for intramolecular dynamics of 92 μs plus a static FRET state. (B) CaM in low-Ca^{2+} buffer. The global fit in this case incorporates two static FRET states but no intramolecular dynamics. Fitting parameters are given in Table 2. (C) Normalized correlations (with triplet dynamics removed) for CaM-AF488-TR in high-Ca^{2+} buffer. $G_{GG}(\tau)$, $G_{RR}(\tau)$, $G_{GR}(\tau)$, and $G_{RG}(\tau)$ are shown as black, red, green, and blue lines, respectively. The arrow points to the shift between the autocorrelation and the cross-correlation curves showing the presence of intramolecular dynamics. (D) Normalized correlations (with triplet dynamics removed) for CaM-AF488-TR in low-Ca^{2+} buffer. The close overlap between autocorrelation and cross-correlation decays shows that no intramolecular dynamics are detected for apoCaM.

TABLE 2: Fitting Parameters for CaM 34-110 in High and Low Ca^{2+} Buffers[a]

fit parameter	high Ca^{2+}[d]	low Ca^{2+}[d]
$\langle N \rangle$	3.13 ± 0.02	2.37 ± 0.02
f_T (green)	0.1	0.1
τ_T (green) (μs)	8	8
f_T (red)	0.09	0.09
τ_T (red) (μs)	18	18
τ_D (μs)[b]	281 ± 6	264 ± 6
τ_D RR (μs)[c]	246 ± 5	247 ± 8
τ_1 (μs)	92^{+170}_{-60}	n.a.
χ^2	1.42	2.53

[a] All fits contained a static FRET component; f_T is the triplet fraction, τ_T is the triplet time constant, and τ_D is the transit time. [b] Transit time for $G_{GG}(\tau)$,$G_{GR}(\tau)$, and $G_{RG}(\tau)$. [c] The transit time for $G_{RR}(\tau)$ was allowed to vary independently to account for photobleaching of the acceptor during transit through the focal volume. [d] Uncertainties were calculated by the support plane method with confidence range 1σ.

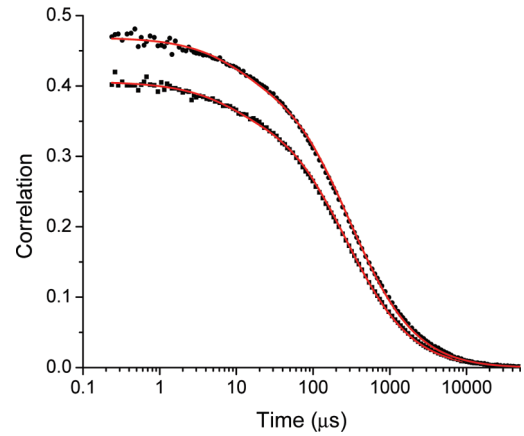

Figure 4. CaM-AF488-AF488 autocorrelation functions in high-Ca^{2+} buffer (circles) and in low-Ca^{2+} buffer (squares). The red lines show fits to eq 2 with triplet correction with $\tau_D = 297 \pm 10$ μs, $f_T = 0.10 \pm 0.02$, and $\tau_T = 8 \pm 3$ μs in the high-Ca^{2+} buffer and $\tau_D = 267 \pm 8$ μs, $f_T = 0.10 \pm 0.02$, and $\tau_T = 8 \pm 3$ μs in the low Ca^{2+} buffer.

target domain are manifested by CaM even when no target domain is present. Because CaM recognition of target polypeptides is controlled by Ca^{2+} binding, understanding the effect of Ca^{2+} on CaM conformational dynamics is necessary for a full understanding of CaM function. The dynamics observed in Ca^{2+}-CaM thus support the notion that the motions required for CaM to function "pre-exist" even in the absence of a substrate.[52,53]

Functionally significant protein dynamics often occur on the microsecond time scale.[54−57] Our goal here is to demonstrate the utility of FCS to detect dynamics on this time scale. Our approach is based on the combination of FCS and FRET. However, the sensitivity of FCS to other dynamic phenomena

on this time scale (triplet dynamics, translational diffusion) means that reliable methods are needed to distinguish dynamic contributions to FCS. The contribution from intramolecular dynamics is distinguishable in FRET FCS because dynamics contribute in a different manner to the autocorrelation and cross-correlation functions, appearing as a decay in the autocorrelations and a rise in the cross-correlations. We use global fitting of the four correlation functions (two autocorrelations and two cross-correlations) from two fluorophores to extract the intramolecular time constants. Control measurements on a system without microsecond dynamics (polyproline) are an important component of our approach. They confirm the validility of the method and, furthermore, allowed determination of triplet parameters that could then be fixed in fits for molecules with dynamics such as CaM. The results presented here also demonstrate the sensitivity of the initial amplitudes of the auto- and cross-correlation functions to the presence of multiple FRET states.

FCS and FRET make a powerful combination as demonstrated in a number of previous investigations. FRET FCS was applied to a fusion protein (called "cameleon"[58]) consisting of cyan fluoroescent protein, CaM, and yellow fluorescent protein. Fitting of the cross-correlation curve yielded a time constant of 42 μs,[42] consistent with the time constant for intramolecular dynamics reported in the present paper. Seidel and co-workers detected submillisecond intramolecular dynamics in a mutant of syntaxin 1 by first finding the diffusion parameters from a mutant that does not show FRET changes and then globally fitting the auto- and cross-correlation curves for a syntaxin mutant exhibiting intramolecular dynamics.[59] In our lab, we previously characterized dynamics in CaM by comparison of the cross-correlation funcion with the autocorrelation function for singly labeled CaM.[20] Recently, in an analysis of intramolecular dynamics in nucleosomes, Torres and Levitus pointed out that intramolecular dynamics could be extracted in the ratio of auto- and cross-correlation functions.[25,60] As an examination of eqs 8−10 shows, the diffusion contribution is thus eliminated and need not be characterized, and as a result, this approach is clearly appealing. However, triplet contributions may also be present in the autocorrelation functions, and these are not elimiated by the ratio method and must therefore be taken into account. We therefore prefer to globally fit the four correlation functions as described in the present paper. Fits to a system without dynamics (polyproline) demonstrate the absence of artifacts and yield the triplet contributions. The global fitting approach has the further advantage of fitting the correlation functions directly, rather than fitting a ratio of two noisy data sets in which taking account of uncertainties in weighted fits could be problematic.

Polyproline. In the absence of intramolecular dynamics, the time dependence of the four correlation functions (after correction for triplet dynamics) is determined by diffusion through the probe volume. The overlap of the four scaled correlation functions in Figure 2 verifies the absence of dynamics and thus the absence of artificats that might be interpreted as dynamics. Thus, the polyproline FRET system can serve as a control for detection of intramolecular dynamics by FRET in FCS measurements. In addition, we can also conclude that segmental motions of the fluorophores themselves, for example, reorientations about their carbon chain linkers or interactions with the protein, do not lead to changes in FRET efficiency on the microsecond to millisecond time scales.

The initial amplitudes depend on the FRET efficiencies (Figure 2). It should be noted that if there is only one FRET efficiency species present in the sample, the initial amplitudes in eqs 5−7 simplify to $1/N_{tot}$ for all of the correlations. This leads to the conclusion that the difference in initial amplitudes demonstrates the presence of multiple FRET states present in the sample, as observed for both polyproline and CaM.

CaM. Comparison of the autocorrelation and cross-correlation curves for CaM at 100 μM Ca^{2+} confirms a contribution from dynamics on the time scale of 100 μs. No contribution from dynamics was detected for CaM at low Ca^{2+} (apoCaM). Static FRET states were also present for both Ca^{2+}-CaM and apoCaM, indicating that FRET states are present that interchange on a time scale longer than the transit time of CaM through the focal volume. We have previously observed FRET states of CaM that interchange on a time scale longer than the transit time.[31,61] The observation of static FRET states may reflect the presence of these conformations.

The 100 μs time scale of dynamics detected by FCS is consistent with other investigations of the dynamics of CaM. Ca^{2+} dissociation in stopped-flow measurements occurs with rates of 240 and 24 s^{-1} (in the presence of 0.1 M KCl), for Ca^{2+} dissociation in the N-terminal and C-terminal domains of CaM, respectively.[62] Nuclear magnetic resonance relaxation measurements of backbone dynamics[63,64] revealed conformational exchange in the C-terminal domain with exchange rates of ∼3000−5000 s^{-1} for CaM at low Ca^{2+} occupancy and exchange contributions of $\sim 2 \times 10^4$ s^{-1} for select residues in apoCaM. However, none of these experimental methods has probed the conformational dynamics within Ca^{2+}-CaM. In experiments with a fast micromixer used to measure the kinetics of Ca^{2+} binding to fluorescently labeled CaM, Ca^{2+} binding was detected on the ∼490 μs and ∼20 ms time scales and attributed to conformational transitions of the C- and N-terminal domains of the protein, respectively.[65] Simulations also have been used to probe conformational dynamics of CaM.[66−68] A study of the N-terminal domain[66] predicted a transition from a closed to open form of the N terminus with a rate of 4×10^4 s^{-1}. The dynamics detected here by FCS for Ca^{2+}-CaM are on a similar time scale and could be related to Ca^{2+} dissociation. However, the fact that dynamics were not detected for apoCaM is inconsistent with an assignment of the dynamics to opening and closing of the Ca^{2+}-binding domains, since these motions are expected in the absence of Ca^{2+}. This suggests that the dynamics detected here by FCS may rather be associated with motions of the N- and C-terminal domains of CaM about the flexible central linker or with global motions within the N-terminal and/or C-terminal domains themselves.

Conclusions

This study presents a global fitting approach to two-color FCS FRET data for both polyproline-AF488-TR and CaM-AF488-TR. The absence of overlap in the initial amplitudes of the four auto- and cross-correlation functions is consistent with the presence of multiple FRET states in the polyproline sample. The overlap of the correlations when normalized to the sample initial amplitude (after correction for afterpulsing and triplet decays) indicated that there were no fluctuations in FRET efficiencies on the time scale of the molecular transit through the excitation volume. Analysis of the auto- and cross-correlation functions confirmed that the difference in initial amplitude is explained by the presence of multiple FRET states in the polyproline peptide.

In this work, FCS was used to measure the dynamics of CaM-AF488-TR with labels at residues 34 and 110. Because FCS FRET experiments can be applied to detect intramolecular dynamics by FRET, our motivation was first to demonstrate

that features or experimental artifacts that might be interpreted as originating from intramolecular dynamics are in fact absent for a system where intramolecular dynamics are not expected. We expect that a system such as polyproline-AF488-TR used here will be useful as a control in studies of intramolecular dynamics by FCS.

For CaM, we detected dynamics with a correlation time of ~90 μs in the presence of Ca^{2+}. The existence of dynamics was demonstrated by the different time dependence of the autocorrelation and cross-correlation functions. Dynamics were not detected for apoCaM. Thus, Ca^{2+} activates CaM intramolecular dynamics. Such motions might be involved in target recognition or binding. The question of the nature of the dynamics requires further investigation by both experimental and computational approaches. The comparison of dynamics detected by FCS for different pairs of labeling sites may further characterize the dynamics and would provide experimental observations for comparison with molecular dynamics simulations.

Acknowledgment. This work was suppported by the National Science Foundation (CHE-0710515). E.S.P. acknowledges support from the Pharmaceutical Aspects of Biotechnology NIH Training Grant (NIGMS 08359).

Supporting Information Available: Details describing burst measurements for Gly-$(Pro)_{15}$-Cys and FCS with three interchanging FRET states. This material is available free of charge via the Internet at http://pubs.acs.org.

References and Notes

(1) Elson, E. L.; Magde, D. *Biopolymers* **1974**, *13*, 1.
(2) Magde, D.; Elson, E. L.; Webb, W. W. *Biopolymers* **1974**, *13*, 29.
(3) Rigler, R.; Widengren, J. *Bioscience* **1990**, *3*, 180.
(4) Rigler, R.; Elson, E. S. *Fluorescence Correlation Spectroscopy: Theory and Applications*; Springer-Verlag: Berlin, 2001.
(5) Hess, S. T.; Huang, S.; Heikal, A. A.; Webb, W. W. *Biochemistry* **2002**, *41*, 697.
(6) Eggeling, C.; Jager, S.; Winkler, D.; Kask, P. *Curr. Pharm. Biotechnol.* **2005**, *6*, 351.
(7) Haustein, E.; Schwille, P. *Annu. Rev. Biophys. Biomol. Struct.* **2007**, *36*, 151.
(8) Widengren, J.; Dapprich, J.; Rigler, R. *Chem. Phys.* **1997**, *216*, 417.
(9) Haupts, U.; Maiti, S.; Schwille, P.; Webb, W. W. *Proc. Natl. Acad. Sci. U.S.A.* **1998**, *95*, 13573.
(10) Lamb, D. C.; Schenk, A.; Rocker, C.; Scalfi-Happ, C.; Nienhaus, G. U. *Biophys. J.* **2000**, *79*, 1129.
(11) Hom, E. F. Y.; Verkman, A. S. *Biophys. J.* **2002**, *83*, 533.
(12) Bonnet, G.; Krichevsky, O.; Libchaber, A. *Proc. Natl. Acad. Sci. U.S.A.* **1998**, *95*, 8602.
(13) Chattopadhyay, K.; Saffarian, S.; Elson, E. L.; Frieden, C. *Proc. Natl. Acad. Sci. U.S.A.* **2002**, *99*, 14171.
(14) Margittai, M.; Widengren, J.; Schweinberger, E.; Schroder, G. F.; Felekyan, S.; Haustein, E.; Konig, M.; Fasshauer, D.; Grubmuller, H.; Jahn, R.; Seidel, C. A. M. *Proc. Natl. Acad. Sci. U.S.A.* **2003**, *100*, 15516.
(15) Koltermann, A.; Kettling, U.; Bieschke, J.; Winkler, T.; Eigen, M. *Proc. Natl. Acad. Sci. U.S.A.* **1998**, *95*, 1421.
(16) Matayoshi, E.; Swift, K. *Springer Ser. Chem. Phys.* **2001**, *65*, 84.
(17) Kohl, T.; Heinze, K. G.; Kuhlemann, R.; Koltermann, A.; Schwille, P. *Proc. Natl. Acad. Sci. U.S.A.* **2002**, *99*, 12161.
(18) Kim, S. A.; Heinze, K. G.; Bacia, K.; Waxham, M. N.; Schwille, P. *Biophys. J.* **2005**, *88*, 4319.
(19) Schwille, P.; Haupts, U.; Maiti, S.; Webb, W. W. *Biophys. J.* **1999**, *77*, 2251.
(20) Slaughter, B. D.; Allen, M. W.; Unruh, J. R.; Urbauer, R. J. B.; Johnson, C. K. *J. Phys. Chem. B* **2004**, *108*, 10388.
(21) Laurence, T. A.; Kapanidis, A. N.; Kong, X.; Chemla, D. S.; Weiss, S. *J. Phys. Chem. B* **2004**, *108*, 3051.
(22) Eggeling, C.; Kask, P.; Winkler, D.; Jaeger, S. *Biophys. J.* **2005**, *89*, 605.
(23) Müller, B. K.; Zaychikov, E.; Brauchle, C.; Lamb, D. C. *Biophys. J.* **2005**, *89*, 3508.
(24) Ruetinger, S.; Macdonald, R.; Kramer, B.; Koberling, F.; Roos, M.; Hildt, E. *J. Biomed. Opt.* **2006**, *11*, 024012/1.
(25) Torres, T.; Levitus, M. *J. Phys. Chem. B* **2007**, *111*, 7392.
(26) Nettels, D.; Hoffmann, A.; Schuler, B. *J. Phys. Chem. B* **2008**, *112*, 6137.
(27) Schuler, B.; Lipman, E. A.; Eaton, W. A. *Nature* **2002**, *419*, 743.
(28) Schuler, B.; Lipman, E. A.; Steinbach, P. J.; Kumke, M.; Eaton, W. A. *Proc. Natl. Acad. Sci. U.S.A.* **2005**, *102*, 2754.
(29) Watkins, L. P.; Chang, H. Y.; Yang, H. *J. Phys. Chem. A* **2006**, *110*, 5191.
(30) Best, R. B.; Merchant, K. A.; Gopich, I. V.; Schuler, B.; Bax, A.; Eaton, W. A. *Proc. Natl. Acad. Sci. U.S.A.* **2007**, *104*, 18964.
(31) Slaughter, B. D.; Allen, M. W.; Unruh, J. R.; Urbauer, R. J. B.; Johnson, C. K. *J. Phys. Chem. B* **2004**, *108*, 10388.
(32) Allen, M. W.; Bieber Urbauer, R. J.; Johnson, C. K. *Anal. Chem.* **2004**, *76*, 3630.
(33) Allen, M. W.; Urbauer, R. J. B.; Zaidi, A.; Williams, T. D.; Urbauer, J. L.; Johnson, C. K. *Anal. Biochem.* **2004**, *325*, 273.
(34) Eid, J. S.; Muller, J. D.; Gratton, E. *Rev. Sci. Instrum.* **2000**, *71*, 361.
(35) Magatti, D.; Ferri, F. *Rev. Sci. Instrum.* **2003**, *74*, 1135.
(36) Wahl, M.; Gregor, I.; Patting, M.; Enderlein, J. *Opt. Express* **2003**, *11*, 3583.
(37) Felekyan, S.; Kuehnemuth, R.; Kudryavtsev, V.; Sandhagen, C.; Becker, W.; Seidel, C. A. M. *Rev. Sci. Instrum.* **2005**, *76*, 083104/1.
(38) Zhao, M.; Jin, L.; Chen, B.; Ding, Y.; Ma, H.; Chen, D. Y. *Appl. Opt.* **2003**, *42*, 4031.
(39) Widengren, J.; Mets, U.; Rigler, R. *J. Phys. Chem.* **1995**, *99*, 13368.
(40) Wohland, T.; Rigler, R.; Vogel, H. *Biophys. J.* **2001**, *80*, 2987.
(41) Price, E. S. Single-Molecule Spectroscopic Tools for Measuring Microsecond and Millisecond Dynamics of Calmodulin; University of Kansas: Lawrence, KS,2009.
(42) Eid, J. S. Two-Photon Dual Channel Fluctuation Correlation Spectroscopy: Theory and Application. Ph.D. Thesis; University of Illinois: Urbana, IL, 2002.
(43) Magde, D.; Elson, E.; Webb, W. W. *Phys. Rev. Lett.* **1972**, *29*, 705.
(44) Berne, B. J.; Pecora, R. *Dynamic Light Scattering*; Wiley: New York, 1976.
(45) Palmer, A. G., 3rd; Thompson, N. L. *Biophys. J.* **1987**, *51*, 339.
(46) Widengren, J.; Mets, Ü. Conceptual Basis of Fluorescence Correlation Spectroscopy and Related Techniques as Tools in Bioscience. In *Single Molecule Detection in Solution*; Zander, C., Enderlein, J., Keller, R. A., Eds.; Wiley-VCH: Berlin, 2002; p 69.
(47) Slaughter, B. D.; Unruh, J. R.; Allen, M. W.; Urbauer, R. J. B.; Johnson, C. K. *Biochemistry* **2005**, *44*, 3694.
(48) Földes-Papp, Z. *Exp. Mol. Path.* **2007**, *82*, 147.
(49) Means, A. R. *Handb. Cell Signaling* **2004**, *2*, 83.
(50) Yamniuk, A. P.; Vogel, H. J. *Mol. Biotechnol.* **2004**, *27*, 33.
(51) Berggård, T.; Arrigoni, G.; Olsson, O.; Fex, M.; Linse, S.; James, P. *J. Proteome Res.* **2006**, *5*, 669.
(52) Eisenmesser, E. Z.; Bosco, D. A.; Akke, M.; Kern, D. *Science* **2002**, *295*, 1520.
(53) Gsponer, J.; Christodoulou, J.; Cavalli, A.; Bui, J. M.; Richter, B.; Dobson, C. M.; Vendruscolo, M. *Structure* **2008**, *16*, 736.
(54) Frauenfelder, H.; Sligar, S. G.; Wolynes, P. G. *Science* **1991**, *254*, 1598.
(55) Englander, S. W.; Kallenbach, N. R. *Q. Rev. Biophys.* **1983**, *16*, 521.
(56) Wand, A. J. *Nat. Struct. Biol.* **2001**, *8*, 926.
(57) Palmer, A. G., III *Chem. Rev.* **2004**, *104*, 3623.
(58) Miyawaki, A.; Llopis, J.; Heim, R.; McCaffery, J. M.; Adams, J. A.; Ikura, M.; Tsien, R. Y. *Nature* **1997**, *388*, 882.
(59) Margittai, M.; Widengren, J.; Schweinberger, E.; Schroder, G. F.; Felekyan, S.; Haustein, E.; Konig, M.; Fasshauer, D.; Grubmuller, H.; Jahn, R.; Seidel, C. A. *Proc. Natl. Acad. Sci. U.S.A.* **2003**, *100*, 15516.
(60) Gurunathan, K.; Levitus, M. *J. Phys. Chem. B* **2009**, *114*, 980.
(61) Slaughter, B. D.; Bieber-Urbauer, R. J.; Johnson, C. K. *J. Phys. Chem. B* **2005**, *109*, 12658.
(62) Martin, S. R.; Andersson Teleman, A.; Bayley, P. M.; Drakenberg, T.; Forsen, S. *Eur. J. Biochem.* **1985**, *151*, 543.
(63) Malmendal, A.; Evenas, J.; Forsen, S.; Akke, M. *J. Mol. Biol.* **1999**, *293*, 883.
(64) Tjandra, N.; Kuboniwa, H.; Ren, H.; Bax, A. *Eur. J. Biochem.* **1995**, *230*, 1014.
(65) Park, H. Y.; Kim, S. A.; Korlach, J.; Rhoades, E.; Kwok, L. W.; Zipfel, W. R.; Waxham, M. N.; Webb, W. W.; Pollack, L. *Proc. Natl. Acad. Sci. U.S.A.* **2008**, *105*, 542.
(66) Tripathi, S.; Portman, J. J. *J. Chem. Phys.* **2008**, *128*, 205104.
(67) Tripathi, S.; Portman, J. J. *Proc. Natl. Acad. Sci. U.S.A.* **2009**, *106*, 2104.
(68) Yang, C.; Jas, G. S.; Kuczera, K. *J. Biomol. Struct. Dyn.* **2001**, *19*, 247.

JP912125Z